P2.14 CLOSE-RANGE OBSERVATIONS OF A TORNADIC SUPERCELL WITH C-BAND POLARIMETRIC DOPPLER RADAR

MATTHEW R. KUMJIAN[1] AND ALEXANDER V. RYZHKOV[1]
J.L. ALFORD[2], M.KNIGHT[2], AND J.W. CONWAY[3]

(1) CIMMS/OU/NSSL, (2) Enterprise Electronics Corporation, (3) Weather Decision Technologies

1. INTRODUCTION

On 1 March, 2007, a supercell thunderstorm produced a devastating EF-4 tornado in the city of Enterprise, located in Coffee County, Alabama. Amidst the tragic loss of life and property on this day, the Enterprise Electronics Corporation "Sidpol" polarimetric radar, also located in Enterprise, collected the first known data set of a violent tornadic storm at extremely close range (within 5 km) at C band. The data were collected for over an hour, encompassing the times before, during, and after the tornado tore through Enterprise.

In this study, we present an analysis of the polarimetric radar data from this event. In the next section, the synoptic conditions are presented, as is a description of the tornado and the collected data. Section 3 presents the radar data, including a discussion of the pertinent polarimetric signatures and the inferences about storm microphysics that can be made from such features. Because of the nature of short wavelength radar measurements, section 4 is devoted to discussing the special considerations of data at C band, including a recently developed method for the correction of attenuation and differential attenuation. Section 5 presents a discussion of applications for those who use short wavelength radar data operationally, including researchers and broadcast meteorologists.

2. BACKGROUND AND METHODOLOGY

a. Synoptic Overview

An occluding 980 mb surface cyclone is evident in the 1800 UTC surface analysis from the Hydrometeorological Prediction Center (HPC, Figure 1), located over south-central Iowa. The associated warm front is draped across Alabama, from northwest to southeast, extending into the Florida panhandle. This boundary is a focal point for initiating convection in the afternoon. Surface flow is moderately strong (around 20 knots), from the south off the Gulf of Mexico. As evident from the 1800 UTC Tallahassee sounding (Fig. 2), the boundary layer was quite moist, though instability was only moderate (less than 1000 J kg^{-1} of convective available potential energy, or CAPE was present by the 0000 UTC sounding). The vertical wind profile shows very strong directional and speed shear in the lowest several kilometers, favorable for rotating storms. The high-shear, moderately low instability setup is common in cool season tornado outbreaks in the southeast (e.g., Vescio and Thompson 1993; Guyer et al. 2006).

As evident in the 1200 UTC upper-air observations, a negatively-tilted trough is located over the Northern Plains. At 500 mb, a jet stream is seen rounding the base of the trough and serves as upper level dynamical support for severe convection that afternoon as it passes over the Gulf Coast states (Fig. 3). Winds at 1200 UTC over Alabama are already greater than 50 knots and will increase with the approaching jet streak. Further aloft, winds are mainly westerly at nearly 100 knots by 300 mb (not shown). This pattern matches the one presented in Guyer et al. (2006). In fact, the severe weather and tornado threat was forecasted rather well by the Storm Prediction Center, which issued a "High Risk" well in advance of the storms. Convection was fairly widespread and initiated around 1400 UTC, with some storms quickly becoming supercellular in such a strongly sheared environment.

b. The Tornado and its Damage

At 1908 UTC on 1 March, 2007, a supercell thunderstorm produced a tornado, first touching down 2 miles southwest of the Enterprise Municipal Airport, in Coffee County, Alabama. After causing minor damage, the tornado lifted briefly before touching back down on the outskirts of the Enterprise city limits. Once entering the city of Enterprise, it strengthened rapidly. At around 1912 UTC, the Enterprise High School suffered a direct hit and suffered low-end EF-4 damage, with estimated maximum winds near 170 mph. Eight students taking shelter in the hallway were killed as the walls collapsed on top of them. As the tornado continued through Enterprise, a ninth victim was killed as the window she was standing in front of shattered. In addition to the nine fatalities, fifty others were injured. The tornado damage path was approximately 10 miles long, with a maximum width of 300 yards. Estimates place total damage costs over $250 million. Nearly 1,400 homes were damaged by the tornado, and of these 239 were completely destroyed (information from NCDC *Storm Events*).

The same supercell was cyclic, producing another brief tornado (that caused no significant damage) at 1925 UTC, followed by another EF-1 tornado in the neighboring Dale County beginning at 1950 UTC. The present study will analyze the Enterprise, Alabama tornado and thus these later tornado events are beyond the scope of this paper.

Corresponding author address: Matthew Kumjian, CIMMS/NSSL, National Weather Center, 120 David L.Boren Blvd., Norman, OK, 73072. Matthew.Kumjian@noaa.gov

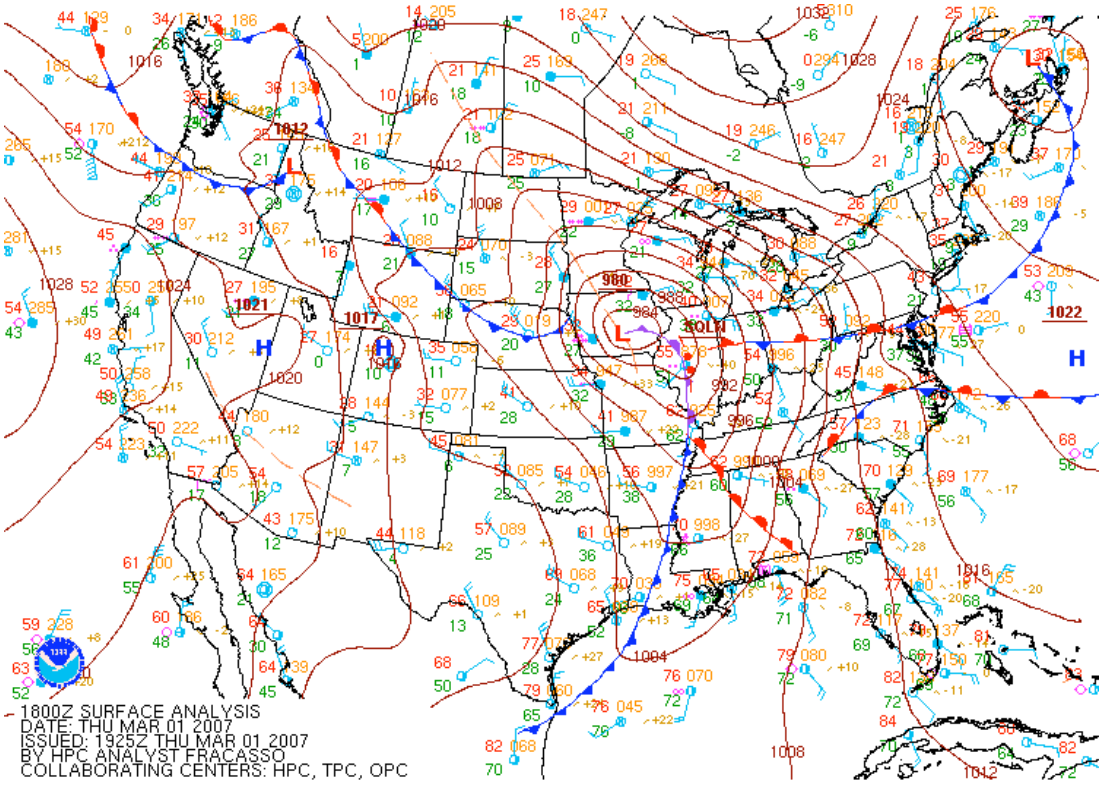

Fig. 1: Surface analysis from 1800 UTC on 1 March 2007. Station observations are plotted along with analyzed synoptic features. Of interest is the deep surface low over Iowa and the associated cold and warm fronts extending southward. Analysis is from the Hydrometeorological Prediction Center (HPC).

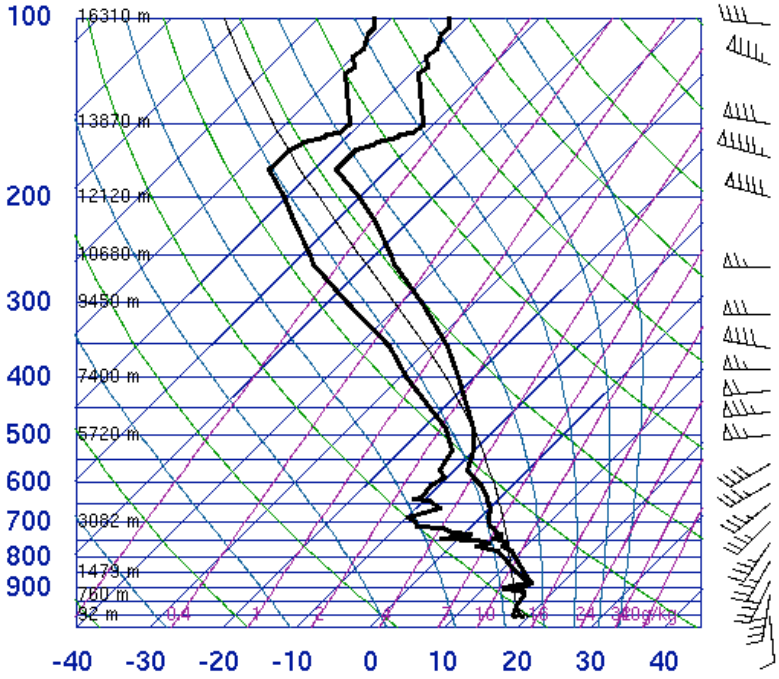

Fig. 2: 1800 UTC sounding from Tallahassee, Florida on 1 March 2007. Notice the strong veering wind shear at low levels, generally moist sounding and low instability. Data from the University of Wyoming sounding archives.

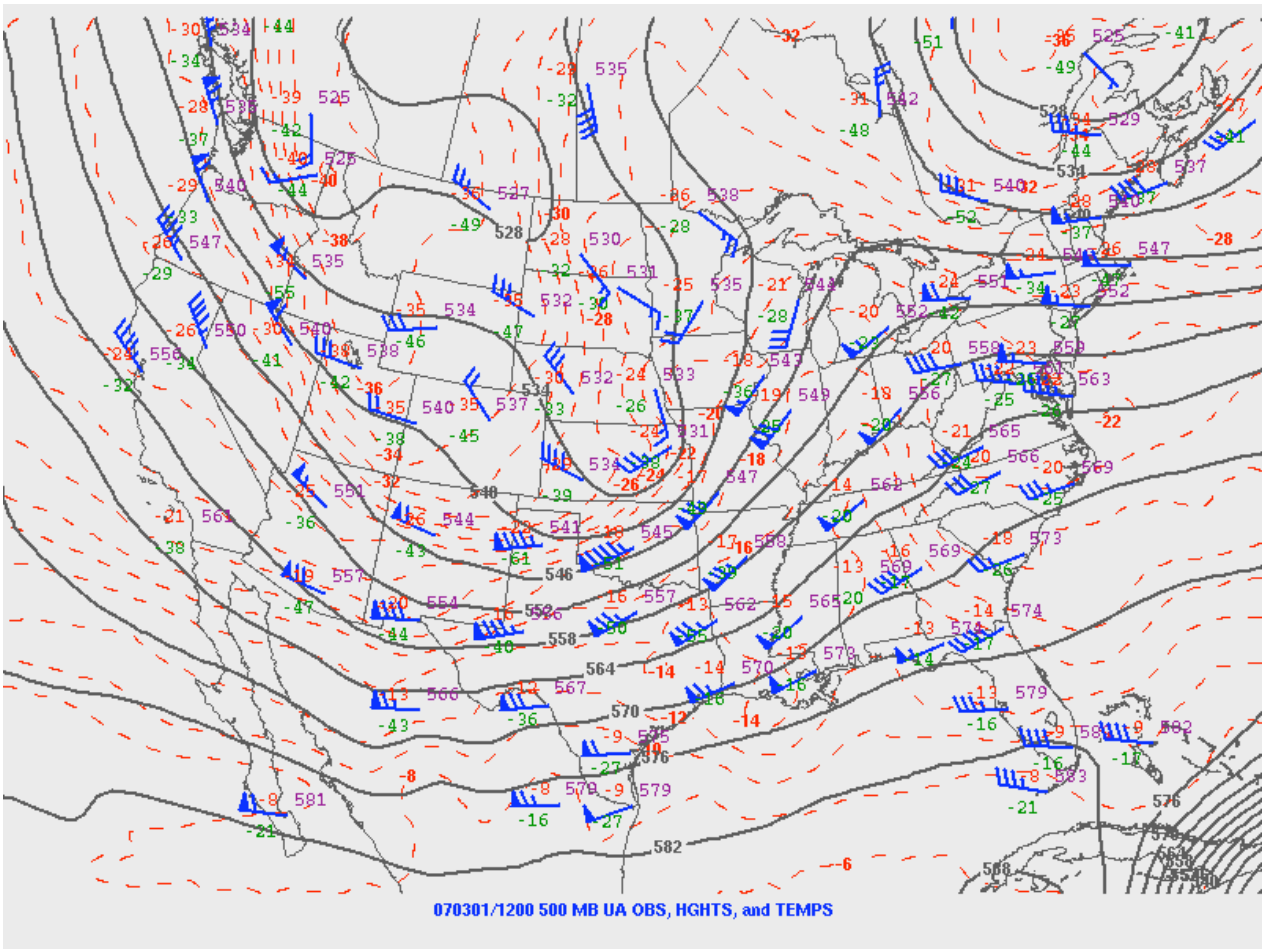

Fig. 3: 500 mb synoptic chart from 1200 UTC on 1 March 2007. A strong negatively-tilted trough is evident over much of the Plains. A jet streak is rounding the base of the trough (over Oklahoma and Texas). Data from the Storm Prediction Center archives.

c. Methodology

The data for this study were collected using the C-band Sidpol polarimetric radar in Enterprise. Data were collected in volume scans consisting of 14 elevation sweeps, ranging from 0.5˚ to 19.5˚. Thus, one volume scan was completed roughly every 7 minutes. Data were collected from 1824 UTC (almost 45 minutes before the tornado) until 1932 UTC, well after the Enterprise tornado dissipated. The tornado passed within 5 km of the radar, providing a high-resolution dataset for the tornado as well as its parent supercell. As the heavy precipitation associated with the forward flank downdraft (FFD) passed directly over the radar, the radar signal suffered severe attenuation and differential attenuation, which is a common problem with short wavelength radar measurements. This problem is addressed later in Section 4. For graphical purposes, the polar surfaces or elevation angle slices are linearly interpolated onto Cartesian grids; the next section presents data in such a manner. The data we present are corrected for attenuation and differential attenuation using the technique described in Section 4.

3. THE DATA

The high-resolution (125 m radial resolution) data collected by the Sidpol radar reveal striking polarimetric features that characterize supercell thunderstorms. These signatures are characteristic of supercells in different climate regions, as first described in Kumjian and Ryzhkov (2007, 2008). Starting at 1824 UTC, two supercell thunderstorms are present within the radar domain, the southern storm producing the eventual Enterprise tornado. At lower levels, the Z_{DR} arc is clearly present in both supercells, with values exceeding 5 dB (Fig. 4a). The Z_{DR} arcs are located at approximately x = -20 km, y = -5 km and x = -35 km, y = -25 km. Being a persistent feature of supercells, the arc is present in every volume scan analyzed for this study with varying degrees of intensity. At midlevels of the southern storm (Fig. 4b), a Z_{DR} ring is evident, as well as a ρ_{HV} half ring. Additionally, the Z_{HH} field shows a bounded weak echo region (BWER). These features indicate rotation may be present at midlevels of the southern storm (Kumjian and Ryzhkov 2007). Figure 5 presents a closer look at these signatures. Also of note

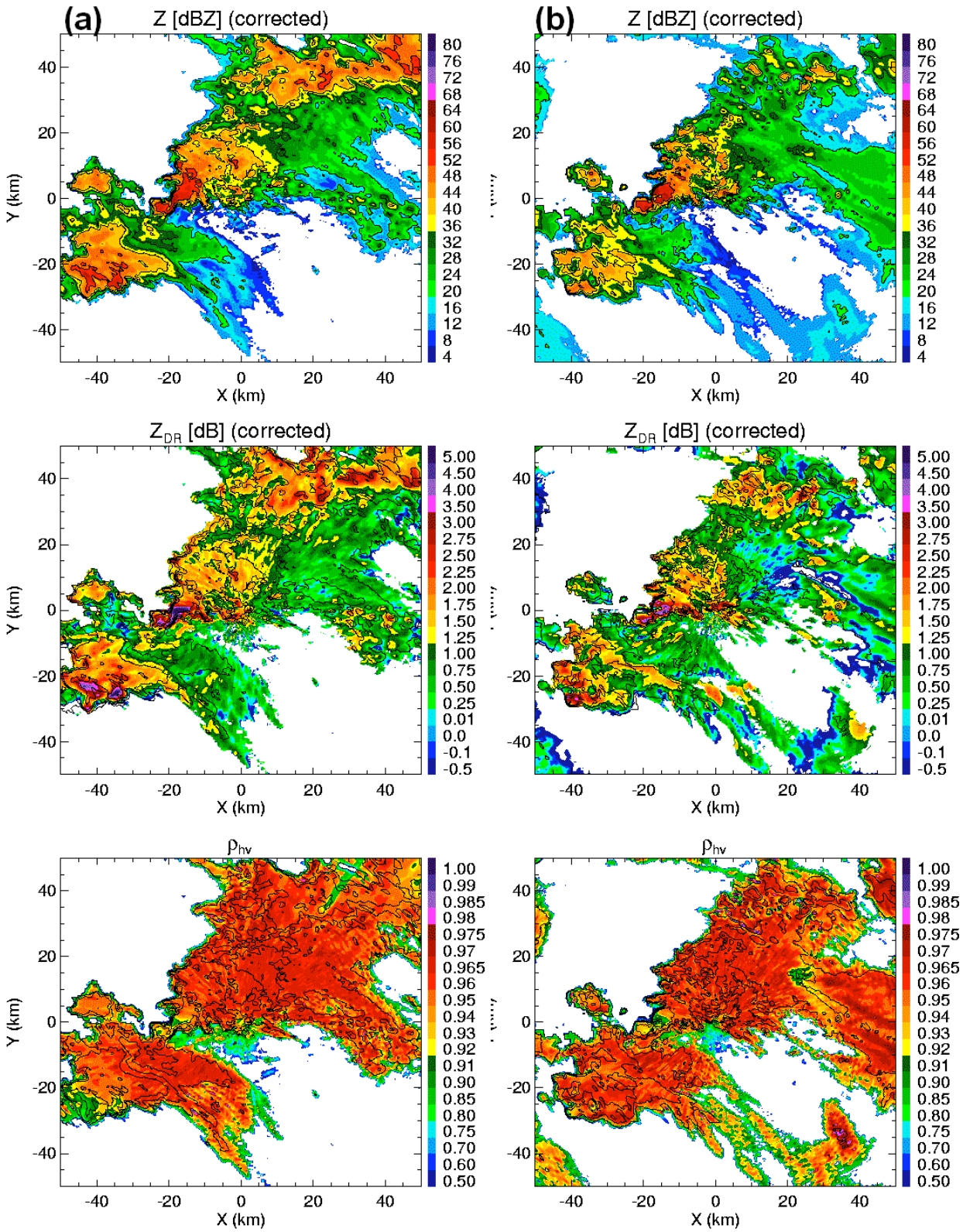

Fig. 4: PPI scans from (a) 1824 UTC at 1.5° elevation and (b) 1827 UTC at 5.5° elevation. The three polarimetric variables shown for each PPI are reflectivity factor at a horizontal polarization (Z_{HH}), differential reflectivity (Z_{DR}), and co-polar cross-correlation coefficient (ρ_{HV}). Of the two supercells present, the Enterprise storm is the one in the southwest portion of the domain. Overlaid are contours of Z_{HH}.

in Figure 4b is the melting layer signature evident in Z_{DR} and ρ_{HV} at a range of about 30 km. The melting layer signature is characterized by an increase in Z_{DR} and a drop in ρ_{HV}. The southern supercell continues to intensify, developing a hook echo in Z_{HH} by 1831 UTC (Fig. 6a). Aloft, the BWER is not as clearly defined. However, the updraft location can be inferred from the depression in ρ_{HV} (Ryzhkov et al. 2005; Kumjian and Ryzhkov 2008), which is attributed to either tumbling hailstones or the ingestion of light debris such as grass, leaves, and insects. Increasing Z_{HH} in the BWER can be an indication of the weakening of the main updraft, which has been associated with tornadogenesis (e.g., Lemon and Doswell 1979).

By 1839 UTC, the Z_{DR} arc is stronger, and the Z_{HH} hook is seen apparently wrapping closer toward the inflow notch (Fig. 6b). Overall, the low level Z_{HH} has increased, signifying heavier precipitation reaching the surface. This could be due to a weakening of the main updraft, often associated with tornadogenesis and is generally considered the most severe stage of the storm (Brandes 1978; Lemon and Doswell 1979; Houze 1993; Adlerman et al. 1999). The low-level inflow signature (Kumjian and Ryzhkov 2008) is present in ρ_{HV}, which also shows a depression associated with the hail core. Note that Z_{DR} does not drop in the hail core as it does in measurements at S band. This will be explained in more detail in the next section. The observations at this time indicate that perhaps the rear-flank downdraft (RFD) is beginning to intensify and spread out over the ground, which sometimes linked to the onset of tornadogenesis. Markowski (2002) provides an excellent review of RFDs and their relation to radar observations of Z_{HH} hook echoes. Doppler velocity data would help confirm this conjecture, but it is not available for this case. No tornado was observed at this time, indicating that any potential tornadogenesis failed. Tornadogenesis failure (Trapp 1999) is further confirmed by the observations at 1847 UTC, which show a less-defined Z_{HH} hook echo and Z_{DR} arc (Fig. 6c). In fact, the low level structure of Z_{HH} and Z_{DR} hint that the mesocyclone may be occluding, or cutting off from the low-level inflow. This is manifest by the inflow notch in Z_{HH} apparently becoming pinched or constricted. Further aloft a Z_{DR} ring is present despite the absence of the BWER. One can infer from this that midlevel rotation is still present, despite the failure of the low-level mesocyclone to intensify to the point of producing a tornado.

At 1900 UTC, the heavy precipitation in the FFD moved directly over the radar, leading to severe attenuation and differential attenuation. The radome became soaked and thus caused another 5 dB attenuation and 0.2 dB differential attenuation. Because of the severe signal loss as well as several bad radials, the data from low levels are difficult to interpret. One noticeable difference from earlier scans is that the hook echo is characterized by higher ρ_{HV} (> 0.90) at this time compared to 1839 UTC. At higher elevation angles, once the storm has moved off the radar, the Z_{HH} hook is very well-defined. The Z_{DR} arc is also strong and exists

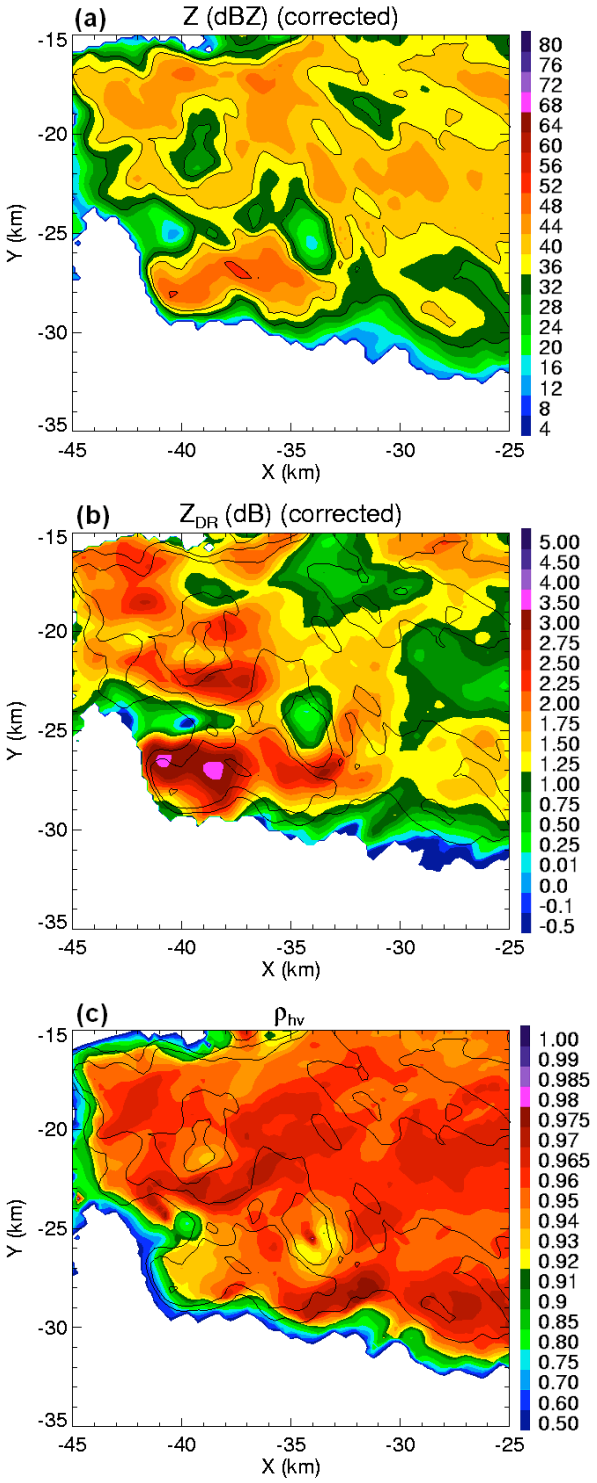

Fig. 5: Same as Fig. 4b, but zoomed in on the midlevel features of the southern storm. The variables shown are (a) Z_{HH}, (b) Z_{DR}, and (c) ρ_{HV}. The BWER and rings are centered on x = −34 km, y = −25 km. Overlaid are contours of Z_{HH}.

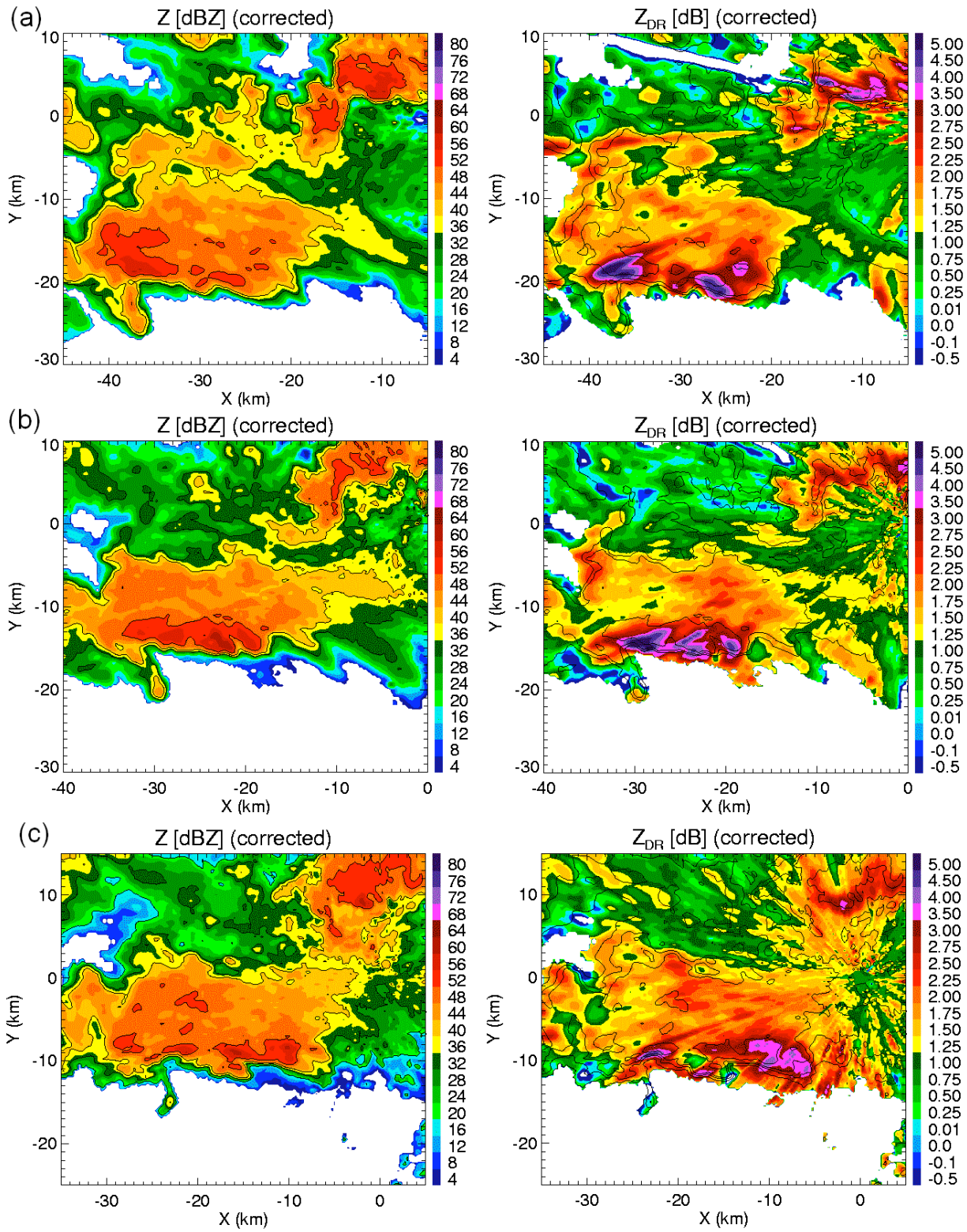

Fig. 6: 0.5° PPI scans of Z_{HH} (left panels) and Z_{DR} (right panels) from (a) 1831 UTC, (b) 1839 UTC, and (c) 1847 UTC. The evolution of the Z_{HH} hook and Z_{DR} arc suggest that the storm underwent tornadogenesis failure during this time period. Overlaid are contours of Z_{HH}.

along the FFD into the inflow region. At further elevation angles still (Fig. 7), an apparent anticyclonic hook or "flare" (Schlatter 2003) is evident at the tip of the hook echo in Z_{HH}. This is indicative of an anticyclonically rotating portion of the downdraft (RFD). Since the RFD is apparently intensifying again, tornadogenesis is possible imminently. Also of note is that the Z_{DR} arc wraps around the hook and curls around in the Z_{HH} weak echo region. This is likely indicative of large liquid drops (ρ_{HV} is still relatively high) and would be visually manifested as a "curtain" of rain wrapping around behind the low-level mesocylcone and wall cloud, an observation frequently made by storm chasers before tornadogenesis.

By 1908, the first tornado touched down just outside of the Enterprise Municipal Airport, where it caused light damage. The polarimetric variables indicate a TDS at this time in the tip of the hook echo (Figure 8). An increase in Z_{HH} (> 50 dBZ), decrease to about 0.25 dB in Z_{DR}, and an anomalously low ρ_{HV} (~ 0.50) are clearly indicative of nonmeteorological scatterers, namely debris lofted by the tornado. All of these observations are consistent with a polarimetric tornadic debris signature (TDS; Ryzhkov et al. 2005; Kumjian and Ryzhkov 2007), which confirms the presence of a tornado on the ground.

The tornado made a direct hit on Enterprise High School at about 1912 UTC. Again, a TDS is clearly visible at the tip of the hook in all three polarimetric variables in Figure 9. The ensuing National Weather Service damage survey on the ground later reported EF-4 damage to the high school at this time. To alleviate some ground clutter, a higher elevation angle was chosen (5.5°). Despite this, the resolution volume is sampling the storm at an altitude of only 300 m, due to the close proximity of the tornado. Thus, the low-level features are still present.

4. SPECIAL CONSIDERATIONS

Polarimetric data at C band requires some special considerations. At these short wavelengths, large raindrops and hailstones are of the size that cause pronounced resonance scattering effects. Additionally, attenuation and differential attenuation are stronger than at S band. Thus, special care should be given to the proper correction of attenuation and interpretation of the measurements. Attenuation correction techniques utilize the fact that Φ_{DP} is immune to attenuation. Earlier simple techniques (e.g., Bringi et al. 1990) make adjustments to Z_{HH} and Z_{DR} by using coefficients of proportionality α and β:

$$\Delta Z_{HH} = \alpha \Phi_{DP} \; ; \Delta Z_{DR} = \beta \Phi_{DP} \qquad (1)$$

The coefficient α is given by:

$$\alpha = \frac{A_H}{K_{DP}} \qquad (2)$$

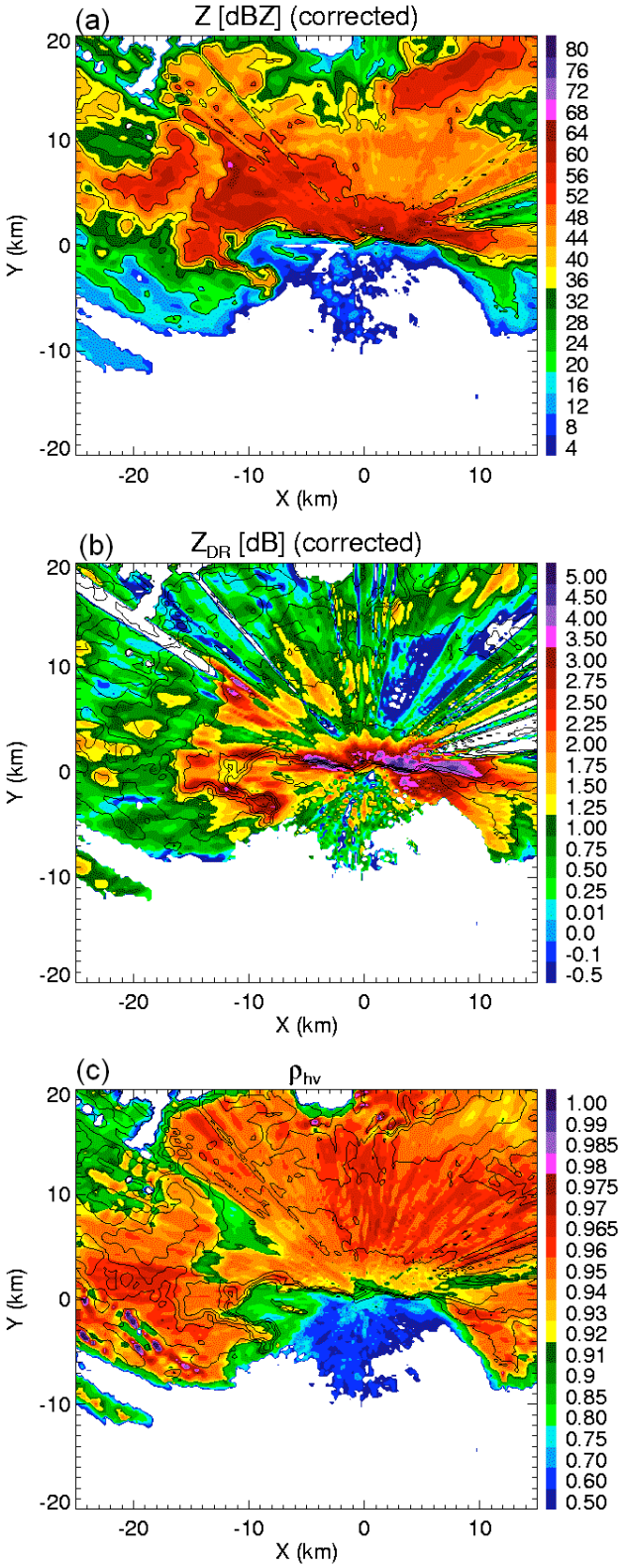

Fig. 7: 6.5° PPI scan from 1904 UTC showing the following corrected variables: (a) Z_{HH}, (b) Z_{DR}, (c) ρ_{HV}. Contours of Z_{HH} are overlaid on each panel (20, 32, 40, and 52 dBZ).

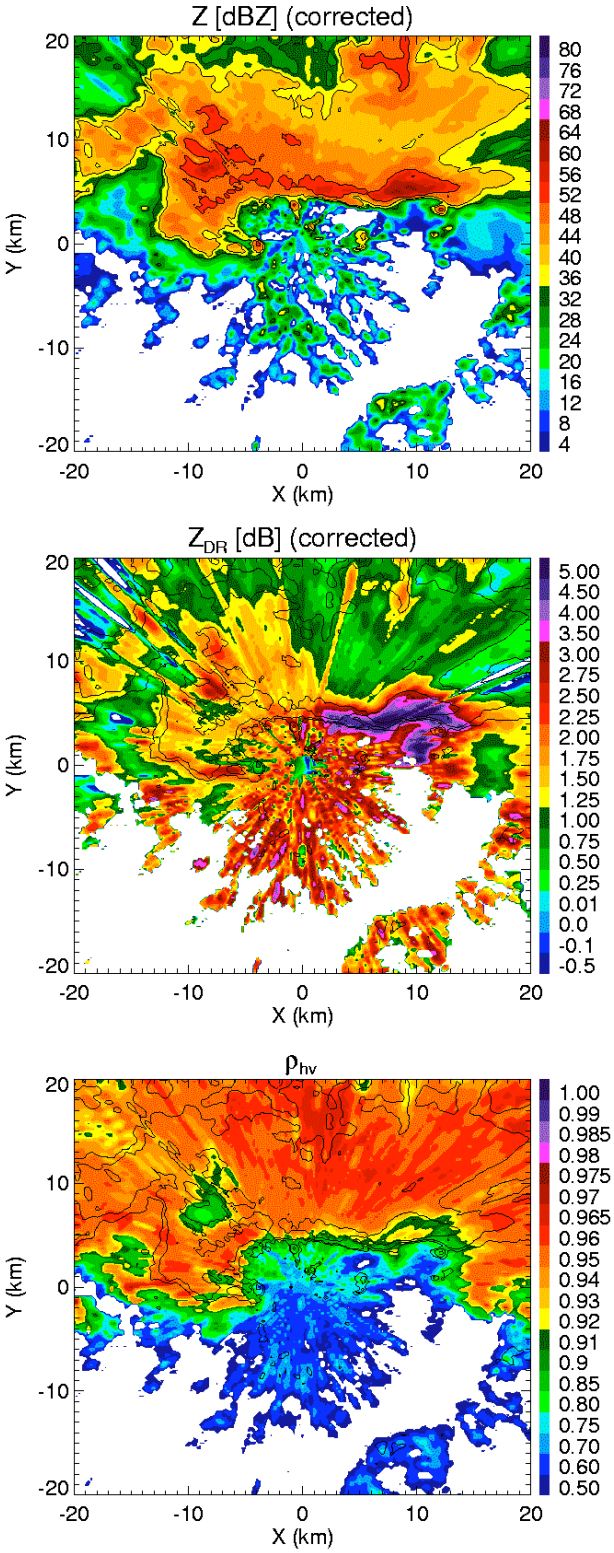

Fig. 8: As in Fig. 7, except from 1908 UTC, showing the 0.5° PPI. A tornadic debris signature (TDS) is evident at the tip of the hook echo, located at about x = −4 km; y = 0 km.

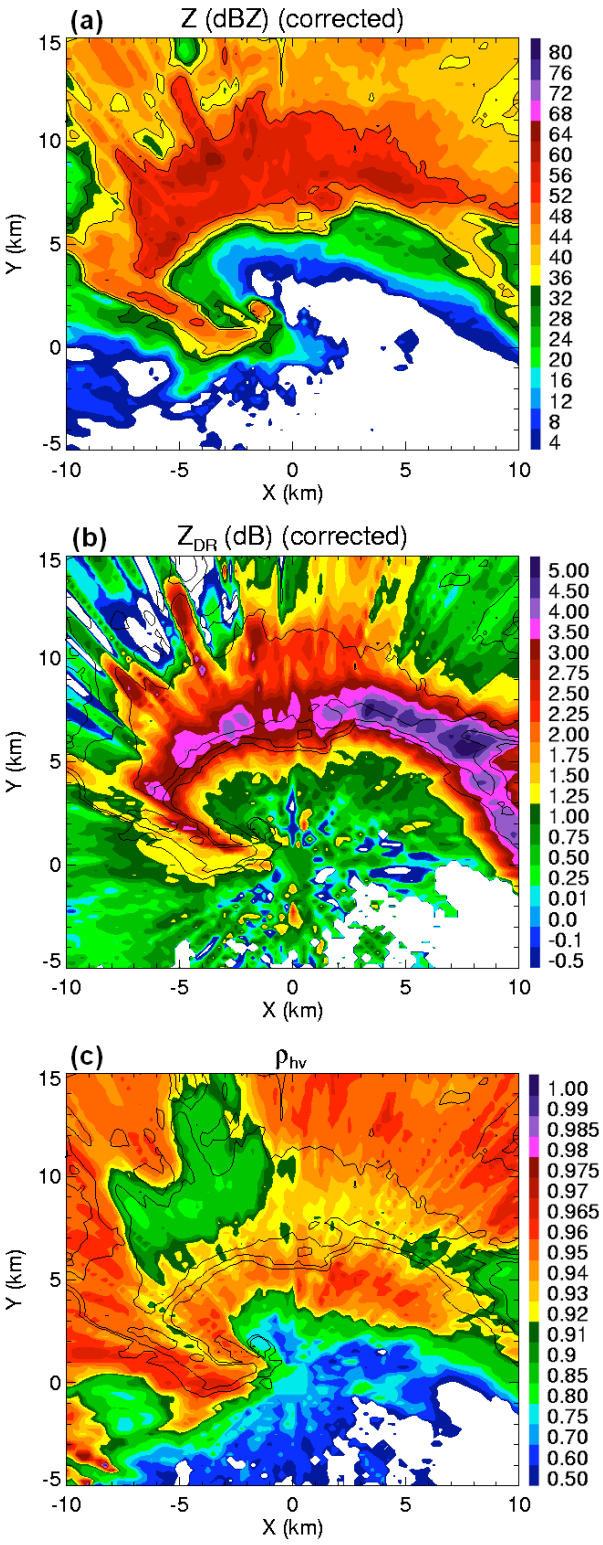

Fig. 9: As in Fig. 8, except from 1912 UTC, showing the 5.5° PPI. A tornadic debris signature (TDS) is evident at the tip of the hook echo, located at about x = −1.5 km; y = 2.0 km. Despite the high elevation angle (5.5°), the radar is sampling the tornado at only about 300 m AGL.

where A_H is the specific attenuation and K_{DP} is specific differential phase, and the coefficient β:

$$\beta = \frac{A_{DP}}{K_{DP}} \tag{3}$$

where A_{DP} is the specific differential attenuation. The proportionality coefficients are assumed generally to not vary much throughout a given storm. However, convective cells with large drops and hailstones can be characterized by significantly varying coefficients, as shown in Ryzhkov et al. (2007b). Various studies attempted to modify the simpler techniques (e.g., Testud et al. 2000; Bringi et al. 2001). However, these do not specifically account for convective cells, which can be quite small in spatial extent but can contribute to a large proportion of the attenuation and differential attenuation within a storm.

Ryzhkov et al. (2006) suggested a new modification to earlier techniques in which α is assumed highly variable in convective cells and is equal to a constant climatological value α_0 outside of such a "hotspot" cell. A "hotspot" is defined as a data bin having Z_{HH} > 45 dBZ when corrected with (1) using $\alpha = \alpha_0$ and ρ_{HV} > 0.80 for at least 2 km of consecutive range gates along a radial (Ryzhkov et al. 2007b). In a "hotspot," $\alpha = \alpha_0 + \Delta\alpha$. Radial profiles of A_H parameterized using $\Delta\alpha$ are computed:

$$A_H(r,\Delta\alpha) = \frac{z_{HH}(r)^b\left[10^{0.1bC}-1\right]}{I(r_0;r_m)+\left[10^{0.1bC}-1\right]I(r;r_m)} \tag{4}$$

where b = 0.8, z_{HH} is the *uncorrected* horizontal reflectivity factor in linear units, the parameter C is given by:

$$C = \alpha_0\Delta\Phi_{DP}(r_0,r_m) + \Delta\alpha\Delta\Phi_{DP}(HS) \tag{5}$$

In (5), the $\Delta\Phi_{DP}(r_0,r_m)$ term is the total increase in Φ_{DP} along the ray where attenuation occurs, and $\Delta\Phi_{DP}(HS)$ is the total increase in Φ_{DP} attributed to the "hotspots." The integral factors in (4) are given as:

$$I(r_0;r_m) = 0.46b\int_{r_0}^{r_m}\left[z_{HH}(s)\right]^b ds \tag{6}$$

and

$$I(r;r_m) = 0.46b\int_{r}^{r_m}\left[z_{HH}(s)\right]^b ds \tag{7}$$

The parameter $\Delta\alpha$ is determined iteratively by satisfying the condition

$$\int_{OHS} A_H(s,\Delta\alpha)ds = \frac{\alpha_0}{2}\Delta\Phi_{DP}(OHS) \tag{8}$$

outside of the hotspots (OHS). Similarly,

$$\Delta\Phi_{DP}(OHS) = \Delta\Phi_{DP}(r_0;r_m) - \Delta\Phi_{DP}(HS) \tag{9}$$

After the above calculations, the corrected Z_{HH} is expressed as

$$Z_{HH}^{(C)}(r) = Z_{HH}(r) + 2\int_{r_0}^{r} A_H(s,\Delta\alpha)\,ds \tag{10}$$

where Z_{HH} is in dBZ and A_H is determined from (8). We also assume that in a hotspot, the proportionality coefficient $\beta = \beta_0 + \Delta\beta$. The Z_{DR} bias at the far side of the attenuating cell is determined as

$$\Delta Z_{DR}(r) = 2\int\beta(s)K_{DP}(s)ds = \beta_0\Phi_{DP}(r) + \Delta\beta\Delta\Phi_{DP}(HS) \tag{11}$$

where

$$\Delta\beta = \frac{Z_{DR}^{(th)} - \min\left[Z_{DR}(r,\beta_0)\right]}{\Delta\Phi_{DP}(HS)} \tag{12}$$

and

$$Z_{DR}(r,\beta_0) = Z_{DR}(r_0) + \beta_0\Phi_{DP}(r) \tag{13}$$

Here, the minimal corrected differential reflectivity beyond a hotspot convective cell ($Z_{DR}^{(th)}$) is between 0.1 and 0.2 dB. This correction technique is validated through extensive tests in Alabama and Canada (Ryzhkov et al. 2007b) and is thus applied to the Enterprise tornado case of this study.

Other factors must be addressed when interpreting C-band polarimetric measurements. Differential phase Φ_{DP} and radar wavelength are inversely related. Thus, smaller wavelength radars will experience a larger Φ_{DP} for a given amount of medium through which the radar beam propagates. Depending on the radar system, Φ_{DP} will "fold" or alias (much like Doppler velocities) at 180° or 360°. Since C-band and X-band radar measured differential phase will increase faster than S-band measurements, the shorter wavelength radars will experience Φ_{DP} folding earlier and more frequently, especially in convective storms and tropical rain environments. Before correcting for attenuation or quantifying rainfall, the measured Φ_{DP} must be properly unfolded.

In addition to Φ_{DP} folding, nonuniform beam filling (NBF) caused by strong gradients of Φ_{DP} impacts small wavelength radar measurements more severely than measurements at S band since Φ_{DP} is inversely proportional to radar wavelength. NBF is manifest in a substantial drop in the observed ρ_{HV} if the gradient of Φ_{DP} becomes too large. Even without the detrimental effects of NBF, the characteristic ρ_{HV} in pure rain at C band can be much lower than at S band. These combined effects produce anomalously low ρ_{HV}, which increases the statistical noisiness of the other measured polarimetric variables (Bringi and Chandrasekar 2001), which can make it difficult to use this variable to distinguish between rain, hail, and nonmeteorological scatterers.

5. DISCUSSION OF C-BAND APPLICATIONS

The previous section illustrated the special considerations required when interpreting short wavelength polarimetric radar data. In the coming years, television stations will undoubtedly begin to incorporate polarimetry into their weather broadcasts in an attempt to stay up to date with the NEXRAD network polarimetric upgrade. Most stations that own or operate a Doppler radar utilize a smaller dish, typically C band. Additionally, multiple research groups at universities and laboratories have developed and are deploying mobile radars for field research. Due to the obvious size constraints, most of these radars are C band or X band. Thus, a growing number of these radars will be used operationally for research or commercial purposes.

Those using such radars need to be especially cautious when interpreting data, especially hydrometeor classifications.

Severe attenuation and differential attenuation at C and X bands can cause serious problems in the radar measurements and subsequently in hydrometeor classification algorithms and should be adequately corrected using a method similar to the one presented in Section 4. If convective precipitation is present in the radar domain and the radar transmits at only one polarization, proper attenuation correction is extremely difficult, and thus quantitative measurements are questionable. If a convective storm is located over the radar, complete signal loss is possible (especially at X band). In this case, attenuation correction is not possible since at least some signal power is required for correction based on Φ_{DP}. Utilization of nearby S-band radars is suggested in this case.

Characteristic polarimetric signatures in convective storms, especially supercells (summarized in Kumjian and Ryzhkov 2008) may be different in C-band observations compared to S-band observations. This is because resonance effects in large raindrops and wet hailstones can also have a significant impact on quantitative measurements at C band. Numerous observations indicate that the Z_{DR} contribution of large raindrops and melting hailstones is overwhelming at C band. Because of this, the intrinsic near-zero Z_{DR} of large tumbling hailstones will be dominated by the very high Z_{DR} of smaller hailstones and raindrops, and the typical hail signature (drop in Z_{DR}) will not occur. This is evident in the analysis of the Enterprise, Alabama tornadic supercell. Throughout the analysis of this storm there is no indication of a decrease in Z_{DR} associated with hail once the data are properly corrected for attenuation. In fact, regions of hail in this storm are marked with anomalously high Z_{DR}. Thus, the fuzzy logic algorithms for hail detection developed for S-band data do not necessarily apply for data from C-band or X-band radars. Kumjian and Ryzhkov (2008) provide a section describing other differences in polarimetric signatures in supercells between S and C bands.

Because ρ_{HV} in pure rain can be considerably lower at C band than at S band, and due to negative ρ_{HV} bias caused by NBF, the polarimetric variables may be plagued with more noise. Polarimetry is incontrovertibly a powerful tool, yet noisy polarimetric variables can be difficult to interpret. Consequently, care must be taken to separate the meaningful microphysical signatures from artifacts or noise.

6. ACKNOWLEDGEMENTS

This work evolved from part of a M.S. Thesis at the University of Oklahoma and is supported under the NSF grant ATM-0532107. Additional funding was provided by NOAA/Office of Oceanic and Atmospheric Research under NOAA-University of Oklahoma Cooperative Agreement #NA17RJ1227, U.S. Department of Commerce. We are grateful for the polarimetric data from Weather Decision Technologies, Inc., and Enterprise Electronics Corporation. Public access to the National Climatic Data Center (NCDC) *Storm Events* data, the University of Wyoming sounding archives, the Storm Prediction Center, and the Hydrometeorological Prediction Center surface analysis archives are also acknowledged.

7. REFERENCES

Adlerman, E.J., K.K. Droegemeier, and R. Davies-Jones, 1999: A numerical simulation of cyclic mesocyclogenesis. *J. Atmos. Sci.*, **56**, 2045-2069.

Brandes, E.A., 1978: Mesocyclone evolution and tornadogenesis: Some observations. *Mon. Wea. Rev.*, **105**, 113-120.

Bringi, V., T. Keenan, and V. Chandrasekar, 2001: Correcting C-band radar reflectivity and differential reflectivity data for rain attenuation: A self-consistent method with constraints. *IEEE Trans. Geosci. Remote Sens.*, **39**, 1906-1915.

Bringi, V. and V. Chandrasekar, 2001: *Polarimetric Doppler Weather Radar*. Cambridge University Press, 636 pp.

Guyer, J. L., D.A. Imy, A. Kis, and K. Venable, 2006: Cool season significant (F2-F5) tornadoes in the Gulf Coast states. Extended Abstracts, 23rd Conf. on Severe Local Storms, St. Louis, MO, Amer. Meteor. Soc., CD-ROM P4.2.

Houze, R.A., 1993: *Cloud Dynamics*. Academic Press, 573 pp.

Kumjian, M.R. and A.V. Ryzhkov, 2007: Polarimetric characteristics of tornadic and nontornadic supercell thunderstorms. Extended Abstracts, 33rd Conf. on Radar Meteorology, Cairns, Australia, Amer. Meteor. Soc., CD-ROM P10.1.

Kumjian, M.R. and A.V. Ryzhkov, 2008: Polarimetric signatures in supercell thunderstorms. *J. Applied Meteor. and Climatology*, accepted.

Lemon and Doswell, 1979: Severe thunderstorm evolution and mesocyclone structure as related to tornadogenesis. *Mon. Wea. Rev.,* **107**, 1184-1197.

Ryzhkov, A.V., T.J. Schuur, D.W. Burgess, and D.S. Zrnic, 2005: Polarimetric tornado detection. *J. Appl. Meteor.*, **44**, 557-570.

Ryzhkov, A.V., D. Hudak, and J. Scott, 2006: A new polarimetric scheme for attenuation correction at C band. Preprints, *4th European Conf. on Radar Meteorology*, Barcelona, Spain, 29-32.

Ryzhkov, A.V., D.S Zrnic, P. Zhang, J. Krause, H. Park, D. Hudak, J. Young, J.L. Alford, M. Knight, and J.W. Conway, 2007a: Comparison of polarimetric algorithms for hydrometeor classification at S and C

bands. Extended Abstracts, *33rd Conf. on Radar Meteorology*, Cairns, Australia, Amer. Meteor. Soc., CD-ROM 10.3.

Ryzhkov, A.V., P. Zhang, D. Hudak, J.L. Alford, M. Knight, and J.W. Conway, 2007b: Validation of polarimetric methods for attenuation correction at C band. Extended Abstracts, *33rd Conf. Radar Meteorology*, Cairns, Australia, Amer. Meteor. Soc., CD-ROM P11B.12.

Testud, J., E. Le Bouar, E. Obligis, and M. Ali-Mehenni, 2000: The rain profiling algorithm applied to polarimetric weather radar. *J. Atmos. Oceanic Technol.*, **17**, 332-356.

Trapp, R.J., 1999: Observations of nontornadic low-level mesocyclones and attendant tornadogenesis failure during VORTEX. Notes and Correspondence, *Mon. Wea. Rev.*, **127**, 1693-1705.

Vescio, M.D. and R.L. Thompson, 1993: Some meteorological conditions associated with isolated F3-F5 tornadoes in the cool season. Preprints, 19th Conf. on Severe Local Storms, Minneapolis, MN, Amer. Meteor. Soc., 2-4.